

Zero-Shot Aerial Object Detection with Visual Description Regularization

Zhengqing Zang^{1,2*}, Chenyu Lin^{1,2*}, Chenwei Tang^{1,2}, Tao Wang^{1,2†}, Jiancheng Lv^{1,2}

¹College of Computer Science, Sichuan University, Chengdu, 610065, P. R. China

²Engineering Research Center of Machine Learning and Industry Intelligence,

Ministry of Education, Chengdu, 610065, P. R. China

{2022223045158, 2022223040017}@stu.scu.edu.cn, tangchenwei@scu.edu.cn, twangnh@gmail.com,

lvjiancheng@scu.edu.cn

Abstract

Existing object detection models are mainly trained on large-scale labeled datasets. However, annotating data for novel aerial object classes is expensive since it is time-consuming and may require expert knowledge. Thus, it is desirable to study label-efficient object detection methods on aerial images. In this work, we propose a zero-shot method for aerial object detection named visual Description Regularization, or *DescReg*. Concretely, we identify the weak semantic-visual correlation of the aerial objects and aim to address the challenge with prior descriptions of their visual appearance. Instead of directly encoding the descriptions into class embedding space which suffers from the representation gap problem, we propose to infuse the prior inter-class visual similarity conveyed in the descriptions into the embedding learning. The infusion process is accomplished with a newly designed similarity-aware triplet loss which incorporates structured regularization on the representation space. We conduct extensive experiments with three challenging aerial object detection datasets, including DIOR, xView, and DOTA. The results demonstrate that *DescReg* significantly outperforms the state-of-the-art ZSD methods with complex projection designs and generative frameworks, e.g., *DescReg* outperforms best reported ZSD method on DIOR by 4.5 mAP on unseen classes and 8.1 in HM. We further show the generalizability of *DescReg* by integrating it into generative ZSD methods as well as varying the detection architecture. Codes will be released at <https://github.com/zq-zang/DescReg>.

Introduction

Aerial object detection aims to detect objects from aerial images (Xia et al. 2018; Yang et al. 2019; Ding et al. 2021), e.g., images captured from an unmanned aerial vehicle (UAV). It plays an important role in many remote sensing applications, such as UAV-aided environmental monitor and disaster response systems. Benefiting from the development of deep convolution neural networks (CNNs), aerial object detection has been extensively studied and advanced (Yang et al. 2019; Zhu et al. 2021; Li et al. 2022, 2020; Deng et al. 2020; Han et al. 2021a) in recent years. Prior research mainly focuses on improving the accuracy or efficiency based on a fully supervised paradigm. However, labeling objects for large-scale aerial images is extremely

*These authors contributed equally.

†Corresponding author

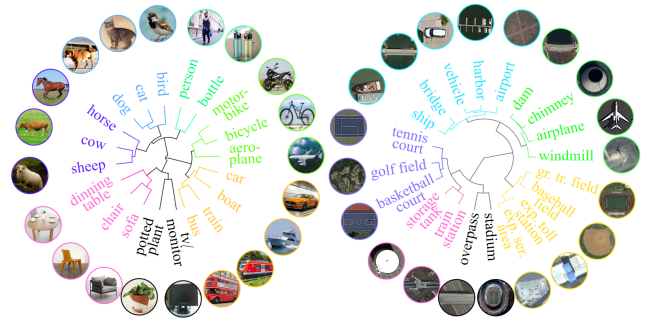


Figure 1: Illustration of weak semantic-visual correlation problem. We perform hierarchical clustering with semantic embeddings and show the radial dendrogram for the 20 common object classes from the Pascal VOC dataset (left) and the 20 aerial object classes from the DIOR dataset(right). The common object classes show clear clustering result which corresponds well to visual appearance (e.g., horse, cow, and sheep), while the semantic clustering of aerial object classes are inevident and shows much less correlation with visual appearance. Best viewed with zoom-in.

costly due to the small object size and irregular viewing angle. Hence expanding the vocabulary becomes a challenge for fully supervised aerial object detection methods (Lam et al. 2018).

Zero-shot object detection (ZSD), which aims to detect unseen object classes without bounding box annotations (Bansal et al. 2018; Demirel, Cinbis, and Ikizler-Cinbis 2018; Rahman, Khan, and Porikli 2018), appears as a promising approach for reducing the copious label demand in aerial object detection. ZSD methods mainly leverage the semantic relation between object classes to detect unseen classes, e.g., Cat and Dog are semantically similar, and thus the knowledge learned on Cat could be transferred to recognize Dog. Methodologically, this knowledge transfer process is typically realized through learning a command embedding function to align visual and semantic features (Rahman, Khan, and Porikli 2018; Bansal et al. 2018; Zheng et al. 2020; Rahman, Khan, and Barnes 2020), or learning a universal synthesizer function to generate training samples (Hayat et al. 2020; Zhao et al. 2020; Zhu, Wang, and

Saligrama 2019; Huang et al. 2022; Sarma, Kumar, and Sur 2022). However, we find that existing ZSD methods perform poorly on aerial images due to weak semantic-visual correlation. Concretely, as shown in Fig. 1, our core observation is that objects in natural images tend to be visually distinct and align well with semantic clustering, yet objects from aerial images often appear vague and lack semantic correlation. Such an issue hinders effective recognition of unseen classes.

Based on the analysis, we aim to introduce additional textual descriptions to augment the semantic space of aerial object classes. These descriptions serve as prior knowledge and provide details on the visual characteristics. One straightforward way to utilize these descriptions is to encode them into semantic embeddings, e.g., through a pre-trained language model. We find such encoding improves the performance but the gain is limited, likely due to the representation gap problem of visual-semantic space (Wang and Chen 2017), which is more severe in aerial images. Based on this finding, we instead leverage the textual description information as a structural regularization and propose a description regularization method, or *DescReg*. The intuition is to preserve the visual similarity structure in the classification space and thus better transfer the knowledge from seen classes to unseen classes. To instantiate the structural regularization, we develop an adaptive triplet loss where each projected class embedding is treated as independent samples. Specifically, the positive pairs are sampled from similar classes, and negative pairs from dissimilar classes. Then the difference between the positive pair and the negative pair is employed as the margin. Such a triplet loss formulation is similarity-aware and helps effectively preserve the inter-class similarity relation in the embedding during optimization.

To validate the above method, we establish two challenging zero-shot aerial object detection setups with DOTA and xView datasets. Together with the existing aerial ZSD setup on the DIOR dataset (Huang et al. 2022), we conduct extensive experiments on the two-stage Faster R-CNN detector and further show generalization the multi-stage Cascaded R-CNN detector (Cai and Vasconcelos 2018) and the popular one-stage YOLOv8 detector (Redmon and Farhadi 2017; Jocher, Chaurasia, and Qiu 2023). *DescReg* effectively improves the detection accuracy of raw baseline method on both seen and unseen classes. Remarkably, *DescReg* with simple one-layer projection outperforms the SOTA generative ZSD methods (Huang et al. 2022) by 4.5 in unseen mAP and 8.1 in HM, with the same detection architecture. We further incorporate our method into the generative ZSD method by regularizing the visual feature synthesizing process and observe significant improvement, which demonstrates the strong generalizability of our *DescReg* as a structural similarity regularization method.

In summary, Our contributions are four-fold:

- To the best of our knowledge, we are the first to conduct a comprehensive study on zero-shot aerial object detection, with in-depth analysis and focused methodological design.
- We identify the weak semantic-visual correlation chal-

lenge in aerial image domain and propose to leverage prior visual text descriptions to address the challenge.

- To effectively incorporate the visual cues conveyed in the textual descriptions, we propose a novel inter-class similarity-aware triplet loss to encode the inter-class relation as a structural regularization.
- We established two new challenging ZSD setups with the DOTA and xView datasets and conduct extensive experiments with various detection architectures to validate and understand the proposed method.

Related Work

Zero-shot Object Detection

Motivated by studies on zero-shot learning (ZSL), which aims to recognise unseen classes by transferring semantic knowledge from the seen ones (Mishra et al. 2018; Tang et al. 2019; Jasani and Mazagonwalla 2019; Demirel, Cinbis, and Ikizler-Cinbis 2019; Tang et al. 2020, 2021), the more challenge task of zero-shot detection (ZSD) proposed in 2018 (Bansal et al. 2018) has received widespread attention recently. The purpose of ZSD is not only to categorize the unseen objects but also localize them. Quite similar to ZSL task, approaches to solving this problem focus on either embedding-based approaches or generative-based approaches. Embedding-based ZSD aims to learn a visual→semantic projection from seen classes to promote the alignment of two spaces (Demirel, Cinbis, and Ikizler-Cinbis 2018; Li et al. 2019b). In order to better distinguish between background and unseen classes, background vector was refined by learnable parameters in (Zheng et al. 2020).

Generative-based methods tackle this problem from the other paradigm (Zhu, Wang, and Saligrama 2019; Zhao et al. 2020). They train a generative adversarial network (GAN) to synthesize visual samples of unseen classes, thereby obtaining unseen classifiers and regressors under supervised paradigms. To maintain inter-class structure and increase intra-class diversity, (Huang et al. 2022) proposed a robust region feature synthesizer with two novel components. For the same purpose, (Sarma, Kumar, and Sur 2022) proposed a triplet loss computed by visual features and added a cyclic consistency loss to constrain visual-semantic alignment. However, none of these methods have recognized the important role of category embedding representation in the performance of ZSD, which is the focus of this study.

Aerial Object Detection

Aerial images refer to images captured by sensors mounted on satellites, aircraft, or drones, which are used to observe and collect information about the Earth’s surface from a distance. Despite the huge progress made in object detection tasks on natural images, the aerial object detection task remains challenging. Prior studies on aerial object detection mainly focus on handling the innate challenge of aerial imagery such as small target size variation (Recasens et al. 2018; Yang et al. 2019; Meethal, Granger, and Pedersoli 2023; Li et al. 2020; Yang, Huang, and Wang 2022; Koyun et al. 2022) and object rotation (Cheng, Zhou, and Han 2016;

Zhang et al. 2020b; Cheng et al. 2019). Despite these efforts, few works study label-efficient detection in aerial images. Some studies (Wolf et al. 2021; Lu et al. 2023) propose few-shot learning approaches for aerial object detection, however, these methods still require target object labels. In this work, we study how to leverage existing training data on seen classes and directly generalize to arbitrary unseen classes, i.e., zero-shot detection.

Proposed Method

Overview

Given the bounding box annotation on a set of seen object categories $\mathbb{F} = \{C_1, C_2, \dots, C_N\}$, zero-shot object detection (ZSD) aims at training on the seen data and generalizing to a set of target unseen object categories $\mathbb{F}^* = \{C_1, C_2, \dots, C_M\}$. In the following paragraphs, we first present our main detection architecture and then introduce our approach with in-depth analyses under the context of ZSD.

Object Detection Architecture The classical two-stage Faster R-CNN (Ren et al. 2015) detection model consists of a visual feature extraction backbone \mathcal{T} , a region proposal network \mathcal{R} , a shared multi-layer feature transformation network \mathcal{F} , a region classifier \mathcal{C} , and a box regressor \mathcal{B} . Given input image \mathbf{I} , the model first extracts image feature \mathbf{F} : $\mathbf{F} = \mathcal{T}(\mathbf{I})$. Then object candidate proposals are predicted by the region proposal network: $\{\mathbf{p}_i\} = \mathcal{R}(\mathbf{F})$. With the proposals, feature pooling is conducted on the image feature map \mathbf{F} to obtain the proposal region feature $\{\mathbf{v}_i\}$. The feature is then further refined by the shared network: $\mathbf{v}_i = \mathcal{F}(\mathbf{f}_i)$. Finally, object classification scores and refined bounding boxes are predicted by the classifier and the regressor: $\mathbf{s}_i = \mathcal{C}(\mathbf{v}_i)$, $\mathbf{b}_i = \mathcal{B}(p_i, \mathbf{v}_i)$.

The detection model can be trained on the seen class data with proposal loss, classification loss, and regression loss: $\mathcal{L} = \mathcal{L}_{prop} + \mathcal{L}_{cls} + \mathcal{L}_{reg}$. The trained region proposal network is class-agnostic and thus may generalize directly to predict the unseen classes. The box regressor is also not sensitive to classes and thus can be applied directly to unseen classes, i.e., by using the class-agnostic version or using prediction from seen classes (Huang et al. 2022). The major challenge here is to generalize the classification to unseen classes, as the region classifier is only trained on the seen class data and cannot predict the unseen classes.

Detecting the Unseen with Semantic Bridging While unseen class data is not available, the semantic relation can be efficiently represented with semantic word embeddings. These embeddings can be obtained from pre-trained word embedding models such as Word2vec (Mikolov et al. 2013) and large language models such as BERT (Devlin et al. 2018): $\mathbf{c}_j = \mathcal{W}(C_j)$, where \mathbf{c}_j is the vectorized representation and \mathcal{W} is the embedding model. With these embeddings and trained detection models on the seen class data, existing zero-shot object detection methods mainly focus on bridging the gap between seen and unseen classes. These methods can be classified into *embedding-alignment* and *generative* methods. The embedding-alignment methods (Khandelwal et al. 2023; Zhang et al. 2020a; Yan et al. 2022)

aim to bridge the gap between visual and semantic space by learning representation alignment. For example, learning an alignment function ϕ to align semantic embeddings to visual features (Zhang et al. 2020a):

$$\mathbf{w}_j = \phi(\mathbf{c}_j) \quad (1)$$

where w_j is the visually-aligned class representation. With w_j , the visual features v_i can be classified based on similarity metrics such as cosine similarity, and the seen classification supervision is employed to learn the alignment function. The learned alignment function is expected to generalize to unseen classes by utilizing unseen class embeddings, and thus the detection model can detect unseen objects.

The Semantic-Visual Correlation Challenge Although such embedding-alignment methods are shown to be effective on natural image datasets such as Pascal (Everingham et al. 2010) and COCO (Lin et al. 2014). They suffer from poor semantic-visual correlation on aerial images: *the semantic embedding c_j has poor correlation with visual features v_i , which leads to severe difficulty for the learned embedding function ϕ to generalize on the unseen classes.* Note this observation also applies to the generative methods which will be discussed in the next section.

Based on this observation, we aim to improve the semantic-visual correlation by augmenting the semantic embeddings with extra visual cues. The visual cues are instantiated as simple textual descriptions. This is motivated by the prior works in zero-shot learning that employs textual descriptions to augment the recognition of unseen classes (Elhoseiny, Saleh, and Elgammal 2013; Paz-Argaman et al. 2020). The descriptions can be obtained from *experts* or simply through large-scale pre-trained *large language models* (LLM), e.g., GPT (OpenAI 2023).

DescReg Formulation

The textual descriptions are free-form and efficient to acquire, they can help provide valuable information such as shape, color, and context for the aerial objects. However, we find simply encoding them into the semantic representation offers limited gain. This is likely due to the following issues: **1)** the representations of semantic feature space and visual feature space have distinct distributions, which causes ineffective transformation of the descriptions into visual feature space. **2)** The image feature representations of aerial objects are less discriminative due to their smaller size than that of common objects, thus it is more difficult to classify them against the false classes and backgrounds.

To address the above issues, we leverage the inter-class visual similarity information as a structural regularization to learn more discriminative alignment functions. Specifically, given the visual descriptions for all seen and unseen classes: $\{T_j\}$, pre-trained language models such as BERT (Devlin et al. 2018) are used to encode them into vectorized representation:

$$\mathbf{t}_j = \mathcal{W}(T_j) \quad (2)$$

where \mathcal{W} is the employed language model and \mathbf{t}_j is the obtained representation. Then we compute the pair-wise cosine

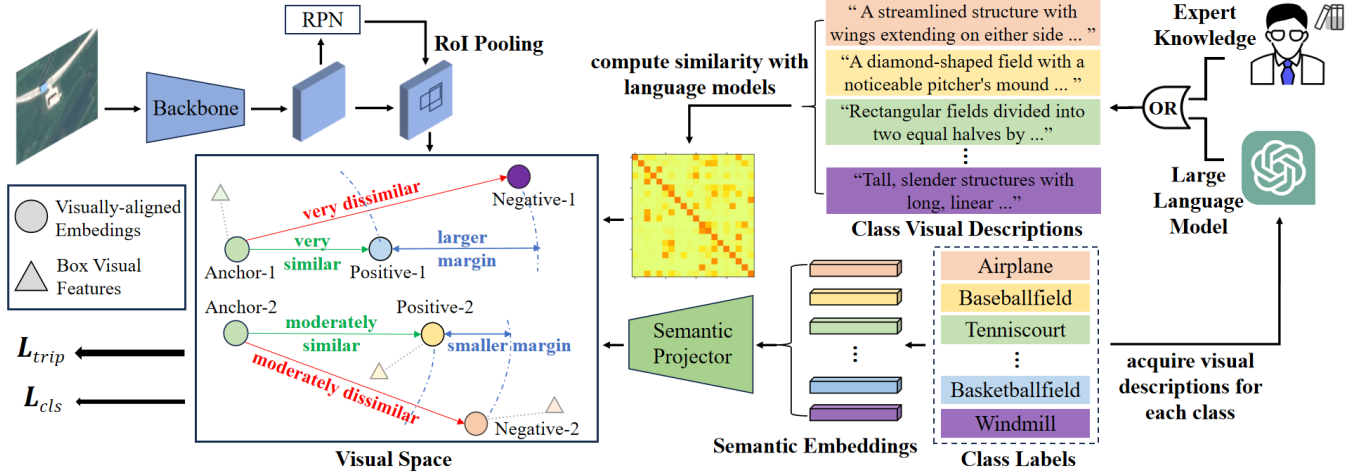


Figure 2: The overall framework of the proposed method.

similarity and obtain the similarity matrix \mathbf{S} :

$$\mathbf{S}(j, k) = \frac{\mathbf{t}_j \mathbf{t}_k}{\|\mathbf{t}_j\|_2 \|\mathbf{t}_k\|_2} \quad (3)$$

To encourage more discriminative inter-class similarity and keep the similarity score within the value range $(0, 1]$, we introduce a self-excluding Softmax:

$$\hat{\mathbf{S}}(j, k) = \begin{cases} \frac{e^{\mathbf{S}(j, k)/\tau}}{\sum_{k' \neq j} e^{\mathbf{S}(j, k')/\tau}} & \text{if } k \neq j \\ \mathbf{S}(j, k) & \text{otherwise} \end{cases} \quad (4)$$

where $\hat{\mathbf{S}}$ is the normalized similarity matrix, of which all the diagonal elements are 1, corresponding to self-similarity and the other elements are in the value range $(0, 1)$, corresponding to inter-class similarity.

The visual characteristics of object classes are now encoded structurally as this similarity matrix. We then integrate it into the embedding alignment learning process. Motivated by the triplet loss (Frome et al. 2013; Akata et al. 2015), we treat the visually-aligned semantic representations \mathbf{w}_j as independent feature samples and perform positive-negative sampling based on the similarity, then triplet loss is imposed on the samples:

$$\mathcal{L}_{trip}^j = \max\{0, d(\mathbf{w}_j, \mathbf{w}_{h(j)}) - d(\mathbf{w}_j, \mathbf{w}_{l(j)}) + \Delta\} \quad (5)$$

where $d(\cdot, \cdot)$ is the Euclidean distance. $h(j)$ denotes sampling a similar class for class j and $l(j)$ means sampling a less similar class, or dissimilar class. The sampling is conducted based on similarity scores $\hat{\mathbf{S}}(j, \cdot)$. Δ is the margin. However, such a direct adoption of triplet loss does not consider the similarity level between classes, e.g., a bridge may be very similar to a dam, but less similar to an overpass, while a vehicle may look a bit dissimilar to a boat but is very distinct to a baseball-field. We thus propose to employ the similarity gap as the margin for the triplet regularization:

$$\Delta_j = \hat{\mathbf{S}}(j, h(j)) - \hat{\mathbf{S}}(j, l(j)) \quad (6)$$

such a second-order metric helps encode the discrepancy in similarity level into the margin regularization. It facilitates the structural learning of the alignment function and thus the knowledge learned from seen classes can better transfer to the unseen classes. The improved similarity-aware triplet loss is thus:

$$\mathcal{L}_{trip}^j = \max\{0, d(\mathbf{w}_j, \mathbf{w}_{h(j)}) - d(\mathbf{w}_j, \mathbf{w}_{l(j)}) + \Delta_j\} \quad (7)$$

Unlike prior works that apply contrastive objectives (Huang et al. 2022; Yan et al. 2022), the proposed margin-adaptive triplet loss is less greedy and allows strong flexibility in representation space. The loss is summed over all the seen and unseen classes to compute the full regularization objective:

$$\mathcal{L}_{trip} = \sum_j \mathcal{L}_{trip}^j \quad (8)$$

During the learning of the alignment function, the classification objective (e.g., cross-entropy) is usually computed on the seen classes. So the complete objective with DescReg is:

$$\mathcal{L} = \mathcal{L}_{cls} + \mathcal{L}_{trip} \quad (9)$$

Fig. 2 shows the overall framework integrated with Faster R-CNN.

Generalization to Generative Methods Unlike the above embedding-alignment methods, the generative methods (Hayat et al. 2020; Zhu, Wang, and Saligrama 2019; Huang et al. 2022; Rahman, Khan, and Barnes 2020) aim to learn universal visual feature synthesizers. The method can be simplified as generating visual feature samples based on semantic embeddings:

$$\hat{\mathbf{v}}_j = \varphi(\mathbf{c}_j, \mathbf{z}) \quad (10)$$

where $\hat{\mathbf{v}}_j$ is the synthesized visual feature and \mathbf{z} is random noise to encourage the feature diversity. The synthesized features can be employed to train the classifier for both seen and unseen classes. Similar to the above-mentioned semantic-visual correlation challenge, here the synthesizer also faces

generalization issues on the unseen classes. The proposed similarity-aware triplet loss can then easily added to the training process of generative networks:

$$\mathcal{L}_{trip}^j = \max\{0, d(\hat{\mathbf{v}}_j, \hat{\mathbf{v}}_{h(j)}) - d(\hat{\mathbf{v}}_j, \hat{\mathbf{v}}_{l(j)}) + \Delta_j\} \quad (11)$$

Experiments

We study four questions in experiments. 1) How does DescReg improve the performance of zero-shot aerial object detection? is it efficient? 2) Is DescReg sensitive to visual descriptions and embedding generation methods? 3) How does each component take effect? 4) Can DescReg generalize to the generative ZSD methods and be applied on different object detection meta-architectures?

Datasets and Experiment Setup

We evaluate the proposed method on three challenging remote sensing image object detection datasets: DIOR (Li et al. 2019a), xView (Lam et al. 2018), and DOTA (Xia et al. 2017). For DIOR, we follow the setting in prior work (Huang et al. 2022). For xView and DOTA, we conduct semantic clustering and sample classes within clusters to ensure unseen class diversity and semantic relatness(Rahman, Khan, and Porikli 2018; Huang et al. 2022). The resulting xView contains 48 seen classes and 12 unseen classes, and the resulting DOTA contains 11 seen classes and 4 unseen classes. We also perform cropping on the xView and DOTA images to simplify the data. Due to space limits, please refer to our supplementary file for more details. Throughout the experiments, unless otherwise stated, we adopt the Faster R-CNN model as the base detection model and IOU=0.5 for the evaluation.

Implementation Details

Following prior works (Yan et al. 2022; Huang et al. 2022; Yan et al. 2022), we adopt Faster R-CNN with ResNet-101 (He et al. 2016) as the base detection architecture and conduct two-stage training. In the first stage, the model is first trained on the seen class data as conventional detection training, In the second stage, the model is frozen and the semantic-visual projection is fine-tuned with the proposed DescReg. In addition to Faster R-CNN, we also validate our method on the newly released one-stage YOLOv8 model (Jocher, Chaurasia, and Qiu 2023) and the cascaded detection model (Cai and Vasconcelos 2018). Due to space limit, please refer to supplementary for more details on implementation.

Main Results

Comparison with State-of-the-arts on DIOR In Tab. 1, we compare the results with state-of-the-art methods on the DIOR dataset. The proposed method outperforms all compared methods in both ZSD and GZSD settings. *Under the ZSD setting*, our method achieves more than 11.0% absolute gain for recalls of different IOU thresholds, and nearly 4.0% mAP increase compared to the best-reported method, demonstrating its much stronger ability to detect unseen categories compared to All other ZSD methods. *Under the*

GZSD setting, the proposed method achieves the best mAP performance on seen classes, surpassing the best-compared method by 11.7% in mAP, this result shows that our zero-shot learning method achieves the least interference on the seen class recognition. Furthermore, our method achieves 7.9% unseen mAP and 14.2% HM, which also significantly outperforms the prior methods. Similar observations hold on the recall metrics.

Experiments on xView and DOTA In addition to DIOR, we further conduct zero-shot detection experiments on the challenging xView and DOTA datasets. We compare to RRFS (Huang et al. 2022) and ContrastZSD (Yan et al. 2022) as representatives of SOTA generative methods and embedding-alignment methods. The result is shown in Tab. 2. On both datasets, our method shows higher performances compared to the baselines. Specifically, Under both ZSD and GZSD settings of xView, the proposed method achieves nearly two-fold improvement in unseen mAP compared to the best-performing ContrastZSD method (4.1% to 8.3%, 2.9% to 5.8%). The corresponding gains on DOTA are about 50% relatively. We also observe that with xView, ContrastZSD achieves similar or higher recalls on the GZSD setting compared to our method, but the unseen mAP is lower, which indicates its unseen images may be less discriminative against the background, and thus predicts more false positives.

Class-wise Results We also report the class-wise mAP performance in terms of ZSD and GZSD for all three aerial object detection datasets. The results are shown in Tab. 3. We note some unseen classes are very challenging and show near 0% AP on the test set (e.g. 0.1% and 0.4% for helicopters on DOTA, under ZSD and GZSD settings respectively). This phenomenon is also observed in prior ZSD works (Yan et al. 2022; Huang et al. 2022; Yan et al. 2022), it is mainly caused by the weak discriminability of unseen class representations and remains a good topic for future ZSD research. Notably, benefiting from the introduced cross-class representation regularization, our method achieves relatively good performances on many unseen classes(e.g. 20.0% GZSD AP and 45.7% ZSD AP for groundtrackfield class on DIOR).

Generalizability

We further validate whether DescReg generalizes to the generative ZSD method and other detection architectures.

DescReg with Generative ZSD Methods Generative methods aim at synthesizing samples for unseen classes, the proposed DescReg can be integrated into the framework for generating more discriminative samples. As shown in Tab. 4, by augmenting with DescReg, the best-reporting generative method of RRFS is improved on PASCAL VOC dataset. Specifically, with DescReg, the mAP performance for unseen classes is improved from 65.5% to 66.4% on ZSD setting, and from 49.1% to 50.4% on GZSD setting.

DescReg with Other Detection Architectures In addition to Faster R-CNN, we further validate DescReg on the one-stage YOLOv8 (Jocher, Chaurasia, and Qiu 2023)

Method	ZSD				GZSD					
	Recall@100			mAP	Recall@100			mAP		
	IoU=0.4	IoU=0.5	IoU=0.6		S	U	HM	S	U	HM
BLC (Zheng et al. 2020)	-	-	-	-	-	-	-	6.1	0.4	0.8
SU (Hayat et al. 2020)	-	-	-	10.5	-	-	-	30.9	2.9	5.3
RRFS (Huang et al. 2022)	-	-	-	11.3	-	-	-	30.9	3.4	6.1
V2S [†] (Khandelwal et al. 2023)	14.1	11.9	10.1	4.1	78.2	15.8	26.3	57.0	1.4	2.7
RRFS [†] (Huang et al. 2022)	22.1	19.8	18.1	9.7	60.0	19.9	29.9	41.9	2.8	5.2
ContrastZSD [†] (Yan et al. 2022)	24.9	22.3	20.1	8.7	69.2	25.9	37.7	51.4	3.9	7.2
DescReg (ours)	37.9	34.6	31.5	15.2	82.0	34.3	48.4	68.7	7.9	14.2

Table 1: Comparison with state-of-the-art methods under ZSD and GZSD settings on DIOR dataset. [†] denotes our implementation results. "S" and "U" denote seen classes and unseen classes, respectively.

Method	xView						DOTA										
	ZSD			mAP	GZSD			mAP	ZSD			mAP	GZSD				
	RE@100	0.4	0.5		0.6	RE@100	S		U	HM	RE@100		0.4	0.5	0.6	RE@100	S
RRFS	17.6	14.3	11.3	2.2	19.1	5.8	8.9	10.2	1.6	2.8	2.9	71.4	14.2	23.7	47.1	2.2	4.2
ContrastZSD	29.0	27.1	25.9	4.1	27.6	13.9	18.5	16.8	2.9	4.9	6.0	69.1	12.2	20.7	41.6	2.8	5.2
DescReg	45.9	43.0	40.1	8.3	28.0	12.8	17.6	17.1	5.8	8.7	8.5	83.8	29.9	44.0	68.7	4.7	8.8

Table 2: Performance of our proposed model on xView and DOTA datasets for ZSD and GZSD settings.

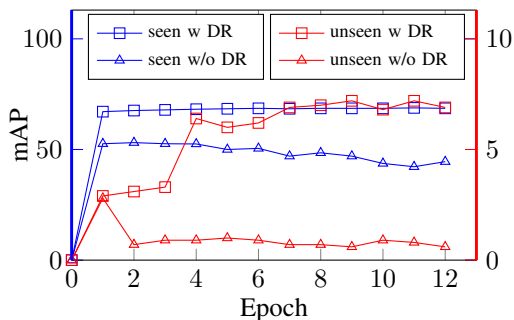


Figure 3: Learning dynamics of DescReg. w/o DescReg denotes DescReg and baseline without DescReg.

and the multi-stage Cascaded R-CNN (Cai and Vasconcelos 2018). The results are shown in Tab. 5. Our method applies well to the two detection models, e.g. with 15.6% ZSD mAP and Cascaded R-CNN and 6.4% ZSD mAP on YOLOv8 which achieves 64 FPS inference speed.

Analysis

We conduct several ablation studies and experimental analyses to better understand how the proposed method works. Please refer to supplementary for qualitative results.

Ablation Study on the Proposed Triplet Loss As shown in Tab. 6, when replacing the semantic class embeddings with the visual description embeddings, the baseline performance is improved but the improvement is limited (e.g., 1.0% on ZSD mAP). This result means naively incorporating the visual description information as the class semantic representation cannot help much due to the representation gap between semantic feature space and visual fea-

ture space. Additionally, by applying the proposed inter-class triplet loss, the performance is significantly improved (from 7.1% to 10.1% on ZSD mAP) which indicates that simple similarity-based triplet regularization could improve the zero-shot detection performance. By further introducing the proposed similarity-aware margin, the ZSD mAP is improved by 5.0% and HM is improved by 5.6%, meaning the adaptive margin helps better regularize the class representation space. We also observe the temperature value of 0.03 achieves the best performance, which is slightly higher than 0.01 and 0.05. Based on the best-performing model, further adding the visual description embeddings cannot offer improvement, indicating our method may already incorporate the visual characteristics into the embeddings through structural similarity regularization. Fig. 3 shows how the learning dynamics of seen and unseen classes, apparently, with DescReg, the performance on both seen and unseen classes are higher and the learning process is more stable.

Effect of Varying Descriptions We investigate how sensitive is DescReg to the input visual descriptions by varying the description sources. We evaluate how different human and GPT-4 (OpenAI 2023) description inputs affect the zero-shot detection performance. As shown in Tab. 7, when focusing on the semantics, the performance of both human and GPT-4 descriptions is low (e.g., 5.0% ZSD mAP for human input and 6.9% mAP for GPT-4 input). The reason is that simple semantic description contains much fewer visual details of the objects. When switching to descriptions that focus on visual details from an aerial view, the performance is significantly improved by more than 8.0% in ZSD mAP and 7.0% in HM, benefiting from the visual details that generate effective similarity measures. We also test how sensitive the method works with different descriptions of varying lengths. The result shows that our method is not very sen-

Setting	Method	DIOR				DOTA				xView											
		airport	bask. f.	gr. tra. f.	windmill	tem. c.	heli.	soccer. field	swim. pool	heli.	bus	pic. track	tru. tra. w/ tox tra.	mar. vessel	motorb.	barge	reach stacker	mobile crane	scraper	excavator	ship. cont.
GZSD	RRFS	3.1	2.0	6.3	0.0	4.4	0.0	4.5	0.0	0.8	2.0	0.0	0.0	3.9	5.5	5.2	0.1	0.0	1.1	0.0	0.4
	ContrastZSD	5.2	2.1	8.1	0.0	3.5	2.9	4.8	0.0	8.1	5.5	0.1	1.2	6.3	9.7	1.2	0.0	0.0	0.1	3.1	0.0
	DescReg	0.0	9.2	20.0	2.4	9.1	0.1	9.5	0.0	21.9	4.5	0.0	6.1	13.3	9.1	8.2	0.0	0.0	0.4	6.1	0.0
ZSD	RRFS	12.3	6.2	19.7	0.6	5.4	0.1	6.1	0.0	0.1	2.4	0.0	0.1	6.9	1.5	9.2	0.5	0.0	5.1	0.0	0.0
	ContrastZSD	9.7	3.9	21.2	0.1	7.4	4.5	11.9	0.0	14.1	5.7	0.0	2.8	7.3	9.7	1.1	0.1	0.0	0.6	7.6	0.0
	DescReg	0.1	10.9	45.7	3.9	11.3	0.4	22.2	0.1	36.0	4.9	0.1	7.5	19.8	9.1	10.2	0.0	0.4	0.9	10.3	0.0

Table 3: Class-wise AP comparison of different methods on unseen classes of three aerial image datasets.

Method	ZSD	GZSD		
		S	U	HM
SAN (2018)	59.1	48.0	37.0	41.8
HRE (2018)	54.2	62.4	25.5	36.2
BLC (2020)	55.2	58.2	22.9	32.9
RRFS (2022)	65.5	47.1	49.1	48.1
RRFS w/. DescReg	66.4	47.1	50.4	48.6

Table 4: ZSD and GZSD performance of the generative method on the PASCAL VOC dataset.

Architecture	ZSD	GZSD			FPS
		S	U	HM	
Faster-RCNN	15.2	68.7	7.9	14.2	11
Cascaded-RCNN	15.6	70.0	8.1	14.5	8
YOLOv8-s	6.4	49.9	4.2	7.7	64

Table 5: Performance with different detection architectures on the DIOR dataset. FPS denotes frame per seconds.

sitive to the description length. In addition, we observe that GPT-generated descriptions offer higher performance than that of human inputs. While we did not dedicatedly optimize the human input, the result shows the application of large language models in ZSD is very efficient.

Conclusion

In this paper, we investigate the zero-shot object detection (ZSD) problem in the context of aerial images. We identified the weak semantic-visual correlation problem of aerial objects and propose to learn stronger visually-aligned class representations with external visual descriptions in text format. Our method is extensively validated on three challenging aerial object detection datasets and shows significantly improved performance to the prior ZSD methods. To the best of our knowledge, we are the first to conduct a comprehensive study on zero-shot aerial object detection. we hope our method and newly established experimental setups provide a baseline for future research.

Limitations and Future Work While our method significantly improves the baselines, we note the performance on unseen classes is still low. The major challenge arises from the strong inter-class confusion and background confusion

S→V	Desc-Softmax	Desc-Adaptive Margin	ZSD	HM
			6.1	5.3
✓			7.1	5.9
	✓(0.03)		10.1	8.2
	✓(0.01)	✓	15.1	13.8
	✓(0.03)	✓	15.2	14.2
	✓(0.05)	✓	14.5	13.6
✓	✓(0.03)	✓	15.3	13.9

Table 6: Ablation study of the proposed similarity-aware triplet loss. S→V means replacing the semantic embeddings with visual description embeddings. Desc-Softmax and Desc-Adaptive-Margin denote the proposed self-excluding Softmax and the similarity-aware triplet loss. The numbers in the parentheses are the temperature used in the Softmax.

-	Method	ZSD	HM
Human	semantic	5.0	4.7
	aerial	13.1	11.9
GPT-4	semantic	6.9	6.1
	aerial-long	15.2	14.2
	aerial-medium	15.1	13.9
	aerial-short	13.5	13.2

Table 7: Varying descriptions. We acquire visual descriptions through both Human and GPT-4. *semantic* means simply describing the object class while *aerial* means focusing on the visual appearance in aerial images. *long*, *medium*, and *short* denote descriptions with varying lengths.

among aerial objects, which is further exacerbated by the small object size. While our method mitigates these problems, two future directions could further address them: 1) The non-uniform spatial processing approaches (Recasens et al. 2018; Yang et al. 2019) could be explored to amplify the small object signal for improved zero-shot recognition. 2) Based on our proposed regularization, other label-efficient methods could be incorporated to improve the performance, e.g. few-shot approach and open-vocabulary detection approach (Kang et al. 2019; Wang 2023).

Acknowledgments

This work is supported by the Key Program of National Science Foundation of China under Grant 61836006, the Fundamental Research Funds for the Central Universities under Grant YJ202342 and 1082204112364, the National Science Foundation of China under Grant 62106161, the Key R&D Program of Sichuan Province under Grant 2022YFN0017 and 2023YFG0278 and Engineering Research Center of Machine Learning and Industry Intelligence, Ministry of Education.

References

- Akata, Z.; Perronnin, F.; Harchaoui, Z.; and Schmid, C. 2015. Label-embedding for image classification. *IEEE transactions on pattern analysis and machine intelligence*, 38(7): 1425–1438.
- Bansal, A.; Sikka, K.; Sharma, G.; Chellappa, R.; and Divakaran, A. 2018. Zero-Shot Object Detection. In *European Conference on Computer Vision*.
- Cai, Z.; and Vasconcelos, N. 2018. Cascade r-cnn: Delving into high quality object detection. In *Proceedings of the IEEE conference on computer vision and pattern recognition*, 6154–6162.
- Cheng, G.; Han, J.; Zhou, P.; and Xu, D. 2019. Learning Rotation-Invariant and Fisher Discriminative Convolutional Neural Networks for Object Detection. *IEEE Transactions on Image Processing*, 28: 265–278.
- Cheng, G.; Zhou, P.; and Han, J. 2016. Learning Rotation-Invariant Convolutional Neural Networks for Object Detection in VHR Optical Remote Sensing Images. *IEEE Transactions on Geoscience and Remote Sensing*, 54: 7405–7415.
- Demirel, B.; Cinbis, R. G.; and Ikizler-Cinbis, N. 2018. Zero-Shot Object Detection by Hybrid Region Embedding. In *British Machine Vision Conference*.
- Demirel, B.; Cinbis, R. G.; and Ikizler-Cinbis, N. 2019. Learning Visually Consistent Label Embeddings for Zero-Shot Learning. *2019 IEEE International Conference on Image Processing (ICIP)*, 3656–3660.
- Deng, S.; Li, S.; Xie, K.; Song, W.; Liao, X.; Hao, A.; and Qin, H. 2020. A global-local self-adaptive network for drone-view object detection. *IEEE Transactions on Image Processing*, 30: 1556–1569.
- Devlin, J.; Chang, M.-W.; Lee, K.; and Toutanova, K. 2018. Bert: Pre-training of deep bidirectional transformers for language understanding. *arXiv preprint arXiv:1810.04805*.
- Ding, J.; Xue, N.; Xia, G.-S.; Bai, X.; Yang, W.; Yang, M. Y.; Belongie, S.; Luo, J.; Datcu, M.; Pelillo, M.; et al. 2021. Object detection in aerial images: A large-scale benchmark and challenges. *IEEE transactions on pattern analysis and machine intelligence*, 44(11): 7778–7796.
- Elhoseiny, M.; Saleh, B.; and Elgammal, A. 2013. Write a classifier: Zero-shot learning using purely textual descriptions. In *Proceedings of the IEEE International Conference on Computer Vision*, 2584–2591.
- Everingham, M.; Van Gool, L.; Williams, C. K.; Winn, J.; and Zisserman, A. 2010. The pascal visual object classes (voc) challenge. *International journal of computer vision*, 88(2): 303–338.
- Frome, A.; Corrado, G. S.; Shlens, J.; Bengio, S.; Dean, J.; Ranzato, M.; and Mikolov, T. 2013. Devise: A deep visual-semantic embedding model. *Advances in neural information processing systems*, 26.
- Han, J.; Ding, J.; Li, J.; and Xia, G.-S. 2021a. Align deep features for oriented object detection. *IEEE Transactions on Geoscience and Remote Sensing*, 60: 1–11.
- Han, Z.; Fu, Z.; Chen, S.; and Yang, J. 2021b. Contrastive Embedding for Generalized Zero-Shot Learning. *2021 IEEE/CVF Conference on Computer Vision and Pattern Recognition (CVPR)*, 2371–2381.
- Hayat, N.; Hayat, M.; Rahman, S.; Khan, S. H.; Zamir, S. W.; and Khan, F. S. 2020. Synthesizing the Unseen for Zero-shot Object Detection. In *Asian Conference on Computer Vision*.
- He, K.; Zhang, X.; Ren, S.; and Sun, J. 2016. Deep residual learning for image recognition. In *Proceedings of the IEEE conference on computer vision and pattern recognition*, 770–778.
- Huang, P.; Han, J.; Cheng, D.; and Zhang, D. 2022. Robust Region Feature Synthesizer for Zero-Shot Object Detection. *2022 IEEE/CVF Conference on Computer Vision and Pattern Recognition (CVPR)*, 7612–7621.
- Jasani, B.; and Mazagonwalla, A. 2019. Skeleton based Zero Shot Action Recognition in Joint Pose-Language Semantic Space. *ArXiv*, abs/1911.11344.
- Jocher, G.; Chaurasia, A.; and Qiu, J. 2023. YOLO by Ultralytics.
- Kang, B.; Liu, Z.; Wang, X.; Yu, F.; Feng, J.; and Darrell, T. 2019. Few-shot object detection via feature reweighting. In *Proceedings of the IEEE/CVF International Conference on Computer Vision*, 8420–8429.
- Khandelwal, S.; Nambirajan, A.; Siddiquie, B.; Eledath, J.; and Sigal, L. 2023. Frustratingly Simple but Effective Zero-shot Detection and Segmentation: Analysis and a Strong Baseline. *arXiv preprint arXiv:2302.07319*.
- Koyun, O. C.; Keser, R. K.; Akkaya, I. B.; and Töreyn, B. U. 2022. Focus-and-Detect: A small object detection framework for aerial images. *Signal Processing: Image Communication*, 104: 116675.
- Lam, D.; Kuzma, R.; McGee, K.; Dooley, S.; Laielli, M.; Klaric, M. K.; Bulatov, Y.; and McCord, B. 2018. xView: Objects in Context in Overhead Imagery. *ArXiv*, abs/1802.07856.
- Li, C.; Yang, T.; Zhu, S.; Chen, C.; and Guan, S. 2020. Density map guided object detection in aerial images. In *proceedings of the IEEE/CVF conference on computer vision and pattern recognition workshops*, 190–191.
- Li, K.; Wan, G.; Cheng, G.; Meng, L.; and Han, J. 2019a. Object Detection in Optical Remote Sensing Images: A Survey and A New Benchmark. *ArXiv*, abs/1909.00133.
- Li, W.; Chen, Y.; Hu, K.; and Zhu, J. 2022. Oriented reppoints for aerial object detection. In *Proceedings of*

- the *IEEE/CVF conference on computer vision and pattern recognition*, 1829–1838.
- Li, Z.; Yao, L.; Zhang, X.; Wang, X.; Kanhere, S. S.; and Zhang, H. 2019b. Zero-Shot Object Detection with Textual Descriptions. In *AAAI Conference on Artificial Intelligence*.
- Lin, T.-Y.; Maire, M.; Belongie, S.; Hays, J.; Perona, P.; Ramanan, D.; Dollár, P.; and Zitnick, C. L. 2014. Microsoft coco: Common objects in context. In *European conference on computer vision*, 740–755. Springer.
- Lu, X.; Sun, X.; Diao, W.; Mao, Y.; Li, J.; Zhang, Y.; Wang, P.; and Fu, K. 2023. Few-shot object detection in aerial imagery guided by text-modal knowledge. *IEEE Transactions on Geoscience and Remote Sensing*, 61: 1–19.
- Meethal, A.; Granger, E.; and Pedersoli, M. 2023. Cascaded Zoom-in Detector for High Resolution Aerial Images. In *Proceedings of the IEEE/CVF Conference on Computer Vision and Pattern Recognition*, 2045–2054.
- Mikolov, T.; Sutskever, I.; Chen, K.; Corrado, G. S.; and Dean, J. 2013. Distributed representations of words and phrases and their compositionality. *Advances in neural information processing systems*, 26.
- Mishra, A.; Verma, V. K.; Reddy, M. S. K.; Subramaniam, A.; Rai, P.; and Mittal, A. 2018. A Generative Approach to Zero-Shot and Few-Shot Action Recognition. *2018 IEEE Winter Conference on Applications of Computer Vision (WACV)*, 372–380.
- OpenAI. 2023. GPT-4. <https://chat.openai.com/>. Accessed: 2024-01-24.
- Paz-Argaman, T.; Atzmon, Y.; Chechik, G.; and Tsarfaty, R. 2020. Zest: Zero-shot learning from text descriptions using textual similarity and visual summarization. *arXiv preprint arXiv:2010.03276*.
- Radford, A.; Kim, J. W.; Hallacy, C.; Ramesh, A.; Goh, G.; Agarwal, S.; Sastry, G.; Askell, A.; Mishkin, P.; Clark, J.; et al. 2021. Learning transferable visual models from natural language supervision. In *International conference on machine learning*, 8748–8763. PMLR.
- Rahman, S.; Khan, S.; and Barnes, N. 2020. Improved visual-semantic alignment for zero-shot object detection. In *Proceedings of the AAAI Conference on Artificial Intelligence*, volume 34, 11932–11939.
- Rahman, S.; Khan, S.; and Porikli, F. 2018. Zero-shot object detection: Learning to simultaneously recognize and localize novel concepts. In *Asian Conference on Computer Vision*, 547–563. Springer.
- Recasens, A.; Kellnhöfer, P.; Stent, S.; Matusik, W.; and Torralba, A. 2018. Learning to zoom: a saliency-based sampling layer for neural networks. In *Proceedings of the European conference on computer vision (ECCV)*, 51–66.
- Redmon, J.; and Farhadi, A. 2017. YOLO9000: better, faster, stronger. *arXiv preprint*.
- Ren, S.; He, K.; Girshick, R.; and Sun, J. 2015. Faster r-cnn: Towards real-time object detection with region proposal networks. In *Advances in neural information processing systems*, 91–99.
- Sarma, S.; Kumar, S.; and Sur, A. 2022. Resolving Semantic Confusions for Improved Zero-Shot Detection. *arXiv preprint arXiv:2212.06097*.
- Tang, C.; He, Z.; Li, Y.; and Lv, J. 2021. Zero-shot learning via structure-aligned generative adversarial network. *IEEE transactions on neural networks and learning systems*, 33(11): 6749–6762.
- Tang, C.; Lv, J.; Chen, Y.; and Guo, J. 2019. An angle-based method for measuring the semantic similarity between visual and textual features. *Soft Computing*, 23: 4041–4050.
- Tang, C.; Yang, X.; Lv, J.; and He, Z. 2020. Zero-shot learning by mutual information estimation and maximization. *Knowledge-Based Systems*, 194: 105490.
- Wang, Q.; and Chen, K. 2017. Zero-shot visual recognition via bidirectional latent embedding. *International Journal of Computer Vision*, 124: 356–383.
- Wang, T. 2023. Learning to detect and segment for open vocabulary object detection. In *IEEE/CVF Conference on Computer Vision and Pattern Recognition*, 7051–7060.
- Wolf, S.; Meier, J.; Sommer, L.; and Beyerer, J. 2021. Double head predictor based few-shot object detection for aerial imagery. In *Proceedings of the IEEE/CVF International Conference on Computer Vision*, 721–731.
- Xia, G.-S.; Bai, X.; Ding, J.; Zhu, Z.; Belongie, S.; Luo, J.; Datcu, M.; Pelillo, M.; and Zhang, L. 2018. DOTA: A large-scale dataset for object detection in aerial images. In *Proceedings of the IEEE conference on computer vision and pattern recognition*, 3974–3983.
- Xia, G.-S.; Bai, X.; Ding, J.; Zhu, Z.; Belongie, S. J.; Luo, J.; Datcu, M.; Pelillo, M.; and Zhang, L. 2017. DOTA: A Large-Scale Dataset for Object Detection in Aerial Images. *2018 IEEE/CVF Conference on Computer Vision and Pattern Recognition*, 3974–3983.
- Yan, C.; Chang, X.; Luo, M.; Liu, H.; Zhang, X.; and Zheng, Q. 2022. Semantics-guided contrastive network for zero-shot object detection. *IEEE Transactions on Pattern Analysis and Machine Intelligence*.
- Yang, C.; Huang, Z.; and Wang, N. 2022. QueryDet: Cascaded sparse query for accelerating high-resolution small object detection. In *IEEE Conference on computer vision and pattern recognition*, 13668–13677.
- Yang, F.; Fan, H.; Chu, P.; Blasch, E.; and Ling, H. 2019. Clustered object detection in aerial images. In *IEEE International conference on computer vision*, 8311–8320.
- Zhang, L.; Wang, X.; Yao, L.; Wu, L.; and Zheng, F. 2020a. Zero-shot object detection via learning an embedding from semantic space to visual space. In *Twenty-Ninth International Joint Conference on Artificial Intelligence*.
- Zhang, Z.; Jiang, R.; Mei, S.; Zhang, S.; and Zhang, Y. 2020b. Rotation-Invariant Feature Learning for Object Detection in VHR Optical Remote Sensing Images by Double-Net. *IEEE Access*, 8: 20818–20827.
- Zhao, S.; Gao, C.; Shao, Y.; Li, L.; Yu, C.; Ji, Z.; and Sang, N. 2020. GTNet: Generative Transfer Network for Zero-Shot Object Detection. *ArXiv*, abs/2001.06812.

Zheng, Y.; Huang, R.; Han, C.; Huang, X.; and Cui, L. 2020. Background Learnable Cascade for Zero-Shot Detection.

Zhu, P.; Wang, H.; and Saligrama, V. 2019. Don't Even Look Once: Synthesizing Features for Zero-Shot Detection. *2020 IEEE/CVF Conference on Computer Vision and Pattern Recognition (CVPR)*, 11690–11699.

Zhu, P.; Wen, L.; Du, D.; Bian, X.; Fan, H.; Hu, Q.; and Ling, H. 2021. Detection and tracking meet drones challenge. *IEEE Transactions on Pattern Analysis and Machine Intelligence*, 44(11): 7380–7399.

Appendix

This appendix is organized as follows:

- In Section A, we provide more dataset details about three remote sensing (aerial) datasets including image cropping, seen/unseen split and evaluation protocols details.
- In Section B, we provide more implementation details of our DescReg model.
- In Section C, we provide additional ablation studies, including the ablation studies of more baselines for DescReg, different projection head architecture, different backbone depth and different embedding methods.

A. More Dataset Details

The details of the three remote sensing (aerial) datasets are as follows:

- **DIOR** (Li et al. 2019a) is a large-scale aerial object detection dataset with large-range object size variation and diverse visual qualities. It consists of 5862 train images, 5863 validation images, and 11725 test images. Total number of classes is 20. The images are in resolution 800x800. Following RRFS (Huang et al. 2022), we employ the combination of train and validation sets to the model and evaluate the model on the test set.
- **xView** (Lam et al. 2018) is a high-resolution aerial object detection dataset, it is collected from WorldView-3 satellites at 0.3m ground sample distance. The resolution is in the range of about 2500x2500 to about 5000x3500 pixels. The dataset consists of 846 annotated images with 60 classes, of which we sample 665 images for training and 181 images for evaluation.
- **DOTA** (Xia et al. 2017) is collected from multiple sensors and platforms such as Google Earth. The resolution is about 800x800 to about 4,000x4,000 pixels. We employ the 1.0 version, which consists of 1411 training images, and 458 validation images. There are 15 categories annotated in the dataset. Models are trained on the train set and evaluated on the validation set.

Image Cropping

For DIOR, we directly employ the images for ZSD experiments following prior work (Huang et al. 2022). For xView and DOTA, due to their varying image size, we simplify the dataset by conducting cropping preprocessing. Each image in the datasets is further cropped into images of size $800 * 800$. Concretely, we crop the image horizontally to $w//800 + 1$ patches. The number of overlapping pixels is $800 + \frac{800-w}{w//800}$, the patches are thus evenly distributed along the width dimension. In practice, we find some of the DOTA images are less than 800 in size, thus if $w \leq 800$, the image is not cropped and we pad the width to 800. The same cropping procedure is done for the image height dimension. With the cropping, we obtain 12826/3549 and 18430/6259 images (training/test) for Xview and DOTA, respectively.

Seen/unseen Split

For DIOR, we follow RRFS (Huang et al. 2022) to split the 20 classes in to 16/4 for seen/unseen classes. For Xview and DOTA, to maintain unseen class diversity (i.e., the unseen classes should be diverse in semantics) and semantic relatedness (i.e., each unseen class should have at least one semantically close seen class.), we perform hierarchical clustering on the class semantic embeddings and sample one class for pairs of leaf nodes in the clustering tree. For example, 'ground-track-field' and 'soccer-ball-field' are clustered together and the soccer-ball-field is sampled as unseen classes. The resulting splits are 11/4 and 48/12 for DOTA and xView respectively. These class splits are:

- **DIOR: seen:** 'airplane', 'baseballfield', 'bridge', 'chimney', 'dam', 'Expressway-Service-area', 'Expressway-toll-station', 'golffield', 'harbor', 'overpass', 'ship', 'stadium', 'storagetank', 'tenniscourt', 'trainstation', 'vehicle', **unseen:** 'airport', 'basketballcourt', 'groundtrack-field', 'windmill'.
- **xView: seen:** 'fixed wing aircraft', 'small aircraft', 'passenger plane or cargo plane', 'passenger vehicle', 'small car', 'utility truck', 'truck', 'cargo truck', 'truck tractor', 'trailer', 'truck tractor with flatbed trailer', 'truck tractor with liquid tank', 'crane truck', 'railway vehicle', 'passenger car', 'cargo car or container car', 'flat car', 'tank car', 'locomotive', 'sailboat', 'tugboat', 'fishing vessel', 'ferry', 'yacht', 'container ship', 'oil tanker', 'engineering vehicle', 'tower crane', 'container crane', 'straddle carrier', 'dump truck', 'haul truck', 'front loader or bulldozer', 'cement mixer', 'ground grader', 'hut or tent', 'shed', 'building', 'aircraft hangar', 'damaged building', 'facility', 'construction site', 'vehicle lot', 'helipad', 'storage tank', 'shipping container', 'pylon', 'tower'. **unseen:** 'helicopter', 'bus', 'pickup truck', 'truck tractor with box trailer', 'maritime vessel', 'motorboat', 'barge', 'reach stacker', 'mobile crane', 'scraper or tractor', 'excavator', 'shipping container lot'.
- **DOTA: seen:** 'plane', 'ship', 'storage-tank', 'baseball-diamond', 'basketball-court', 'ground-track-field', 'harbor', 'bridge', 'large-vehicle', 'small-vehicle', 'roundabout'. **unseen:** 'tennis-court', 'helicopter', 'soccer-ball-field', 'swimming-pool'.

Evaluation Protocols

Same as common ZSD setup (Bansal et al. 2018), we employ Recall@100 (RE@100) and mean average precision (mAP) as the criteria for evaluation with an intersection over union (IoU) of 0.5. In the GZSD setting, the performance is evaluated on both seen and unseen subsets. The Harmonic Mean (HM) (Han et al. 2021b) is used as a final metric to combine seen and unseen performance. For the ZSD setting, we follow prior works (Huang et al. 2022; Yan et al. 2022; Rahman, Khan, and Barnes 2020) and evaluate on test images that only contain unseen classes. For the first 6 unseen classes on Xview (i.e., 'helicopter', 'bus', 'pickup truck', 'truck tractor with box trailer', 'maritime vessel', 'motorboat'), this criterion filters too many images and keeps only

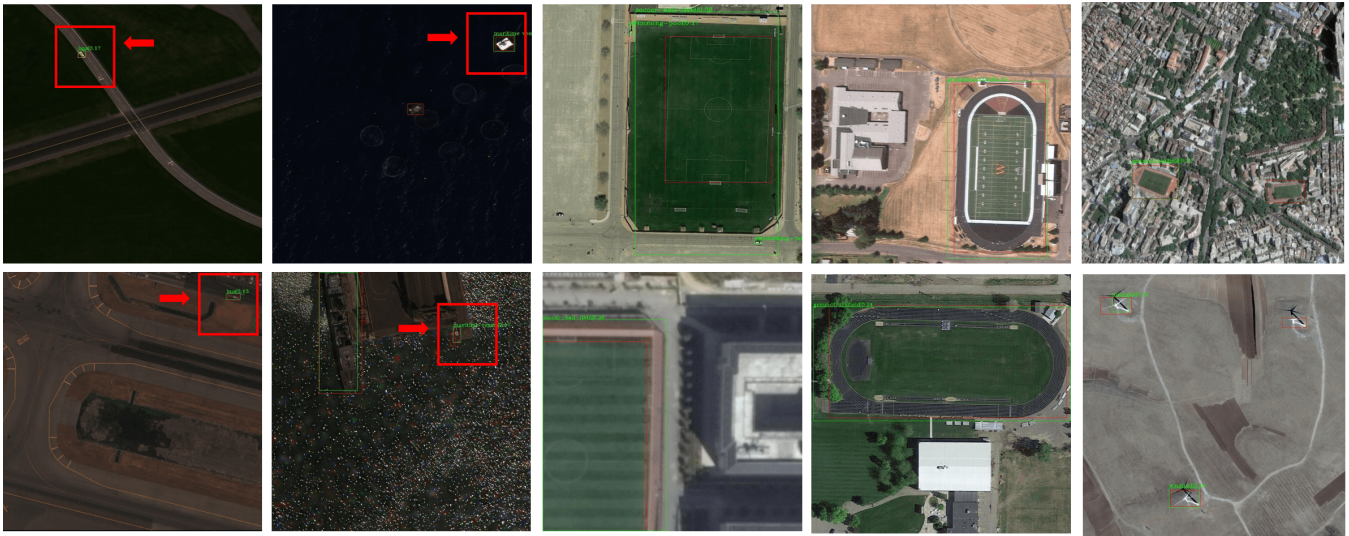


Figure 4: Qualitative results on DIOR, xView and DOTA, for unseen objects. The green are detections and the red are ground-truth boxes. The small results on xView are marked with red anchors. Best viewed with zoom-in.

a few of ground truth, which results in exceptionally high AP results. We thus relax this image selection criterion and include images that contain the least seen class objects for the first 6 unseen classes.

B. More Implementation Details

DescReg Implementation

Training As mentioned in our main paper, we conduct two-stage training: 1) In the first stage, the model is trained on the seen class data, and the training takes 12 epochs on all three datasets, the learning rate is 0.01 with decay at 8th and 11th epochs. We employ SGD with $momentum = 0.9$ and $weight-decay = 0.0001$ as the optimizer. 2) In the second stage, the model is frozen and the classifier layer is replaced with the projection head, the projection head is fine-tuned with DescReg objective, which consists of classification loss and triplet loss. The optimizer detail is the same as the first stage of training, with only a different learning rate of 0.02. For background embedding, We follow the prior work of BLC (Zheng et al. 2020) and employ learnable background representation during the second-stage training.

Implementation on RRFS To incorporate DescReg into RRFS (Huang et al. 2022) and compare with it on the Pascal VOC dataset, we first generate descriptions on the 20 classes with GPT-4 and then follow the same process as on the aerial dataset to compute the triplet loss, the original inter-class contrastive loss in RRFS is then replaced with our triplet objective. The other training sets and hyper-parameters are identical to RRFS.

Implementation on Cascaded R-CNN and YOLOv8 It is very simple to integrate our method into other object detection meta-architectures such as cascaded object detectors and one-stage detection detectors. We employ Cascaded R-CNN (Cai and Vasconcelos 2018) and YOLOv8 (Jocher,

Chaurasia, and Qiu 2023) to validate the generalization on these architectures. For Cascaded R-CNN, after the first stage detection training on seen class data, we replace the classifier of each stage with an independent semantic projection head and conduct fine-tuning with the proposed DescReg. For YOLOv8, unlike Faster R-CNN and Cascaded R-CNN which employ Softmax for classification by default, it uses class-wise Sigmoid loss for classification, we simply replace the logit before Sigmoid activation with dot product similarity between the projected class embeddings and visual features. The training follows the same two-stage fashion as Faster R-CNN and Cascaded R-CNN.

C. Additional Ablation Studies

More Baselines for DescReg

We evaluate some other alternative Design Choices of DescReg as baselines: 1)forcing diagonal similarity matrix in triplet loss regularization, i.e., each class is only similar to itself and is not similar to any other classes (0.0 similarity). In this way, the proposed triplet loss is reduced to an inter-class contrastive loss. 2)direct similarity regularization: we compute cosine embedding similarity and directly impose L2 loss with the similarity computed from the descriptions. As shown in Tab. 8, these two baseline alternative choices generate much worse results compared to the proposed similarity-aware triplet loss formulation. This results shows that our method can more effectively encode the structural inter-class similarity information into the embedding learning and thus achieves better ZSD performance.

Head Architecture

Tab. 9 shows an ablation study on the projection head architecture. We thus employ a 1-layer projection head for DIOR and xView, and a 2-layer projection head for DOTA. The results indicate that DescReg performance depends on the pro-

-	ZSD	HM
proposed	15.2	14.2
diagonal similarity	7.3	6.4
direct similarity reg	8.7	6.2

Table 8: Alternative Design Choices for DescReg. *diagonal similarity* means forcing the similarity matrix as a diagonal eye matrix. *direct similarity reg* denotes imposing L2 loss directly on the cosine similarity computed from the embedding and descriptions.

jection head architecture as well as the dataset. It is better to validate and find the best setting.

-	Arch	ZSD	HM
DIOR	1-fc	15.2	14.2
	2-fc	14.8	13.7
	3-fc	12.5	11.0
DOTA	1-fc	8.0	8.1
	2-fc	8.5	8.8
	3-fc	7.2	7.3
Xview	1-fc	8.3	8.7
	2-fc	7.7	7.5
	3-fc	6.7	6.3

Table 9: Effect of different projection head architecture, if the layer is more than 1, we use intermediate feature dimension of 128. The experiment is conducted on DIOR dataset.

Different Backbone Depth

As shown in Tab. 10, we replace the default ResNet-101 backbone with ResNet-50 and ResNet-152. The results indicate that the performance improves significantly from ResNet-50 to ResNet-101 (e.g., 12.3 to 15.2 in ZSD mAP). However, further increasing the backbone depth to ResNet-152 obtains diminished gain on unseen class detection. While the seen class mAP is improved with the deeper network, the result shows that the unseen class may not benefit further with deeper network representation.

-	seen	ZSD	HM
res-50	60.5	12.3	10.9
res-101	68.7	15.2	14.2
res-152	70.1	15.0	14.4

Table 10: The effect of backbone depth. The experiments are conducted on DIOR dataset. *seen* denotes mAP on seen classes.

Embedding Models We examine the effect of different semantic embedding methods and visual embedding methods. As shown in Tab. 11, we find: 1) For both semantic embeddings and description embeddings, the pre-trained language models such as BERT offer relatively good results,

e.g., 15.2% ZSD mAP with BERT semantic embedding and S-BERT description embedding. 2) The vision-language pre-trained model of CLIP (Radford et al. 2021) can further improve the best-performing language model (e.g., 15.8% vs. 15.2% with CLIP semantic embedding and BERT semantic embedding), this is likely due to the leaked visual cues in the vision-language representation. We mainly adopt pure language models to conform with the zero-shot setting.

-	Method	ZSD	HM
Semantic	Word2Vec (2013)	12.0	11.7
	GloVe (2014)	12.1	10.9
	BERT (2019)	15.2	14.2
	CLIP (2021)	15.8	14.6
Description	BERT (2018)	13.5	13.1
	DSG (2018)	14.9	13.6
	S-BERT (2019)	15.2	14.2
	CLIP (2021)	15.5	14.6

Table 11: Effect of different embedding methods. The results are obtained for semantic class names and visual descriptions independently, i.e., by fixing one and varying the other.

Qualitative Results As shown in Fig. 4 is some example qualitative results, our method can correctly detect some challenging unseen objects such as the windmill, bus, and maritime vessel.